# SSDM2024-121653

# BIOMIMETIC SCALED STRUCTURES - EXPLORING SYMMETRIES AND NONLINEARITY IN STRUCTURAL DAMPING

Md Shahjahan Hossain, Omid Bateniparvar, Pranta Rahman Sarkar, Ranajay Ghosh

Department of Mechanical and Aerospace Engineering
University of Central Florida
Orlando, FL, USA

# **ABSTRACT**

Fish scale-like features on substrates arranged periodically produce peculiar mechanical behavior. These include nonlinear stiffness, anisotropy in deformation, and finally jamming behavior. These smart structures can be fabricated by partially embedding stiffer plate-like segments on softer substrates to create a bi-material system, with overlapping scales. The dynamic response shows remarkable geometrical-material interplay and anisotropies in damping. Especially interesting is the damping behavior that is distinct from typical damping found in mechanical structures which are often approximated as Rayleigh-Damping. Here we discuss some of these dynamic behaviors that include material-geometry distinction in damping, multiple damping scenarios and interplay of dissipation possibilities. We performed experimental analysis and compared the results with simple mathematical laws that govern architecture-dissipation relationships that can help understand the vibrating response of pillar/scale-covered membranes/thin plates. We conclude by noting the applicability these metastructure in structural damping with other forms currently in use in practice.

Keywords: Metamaterial; fish scale; structural dynamics; biomimetics.

# 1 INTRODUCTION

Aerospace structures for novel applications such as eVTOL (as shown in Fig. 1), and micro UAVs require smart materials to maintain flexibility and favorable aerostructural characteris-

tics [1, 2, 3]. These smart structures can also be protected from low-velocity impacts and various other loading conditions incorporating different type symmetric and assymetic metamaterial structure based on the requirement. They demonstrate dynamic responses to changes in acceleration, temperature, humidity, etc and Inspired by biological systems, they efficiently distribute loads and offer effective impact resistance. Membranes or thin plates, characterized by their flexibility, lightweight nature, and structural versatility, have a wide range of applications in various fields, including aerospace, civil engineering, and advanced materials, etc [2,4]. Thus, the exploration of membrane and thin plate applications in the context of impact loading becomes increasingly relevant.

The vibration of membranes and thin-plate structures has consistently fascinated researchers over the years and many researchers have focused on analyzing membrane vibrations and analytically studying the free vibration of thin rectangular membranes [8] [9, 10, 11]. Several studies were done to analyze the dynamic response of different types of membrane structures [12, 13, 14]. Abdulkerim et al. (2019) experimentally analyzed the nonlinear vibration of thin rectangular aluminum alloy plate [15] and Lu et al. (2023) analyzed free vibration analysis of Bio-Inspired carbon fiber reinforced polymer composite laminated plates [16]. Several additional studies have underscored the promising applications of high-speed cameras and digital image correlation (DIC) in the realm of vibration analysis and damping measurements. These investigations collectively contribute to the growing body of research exploring the potential of these

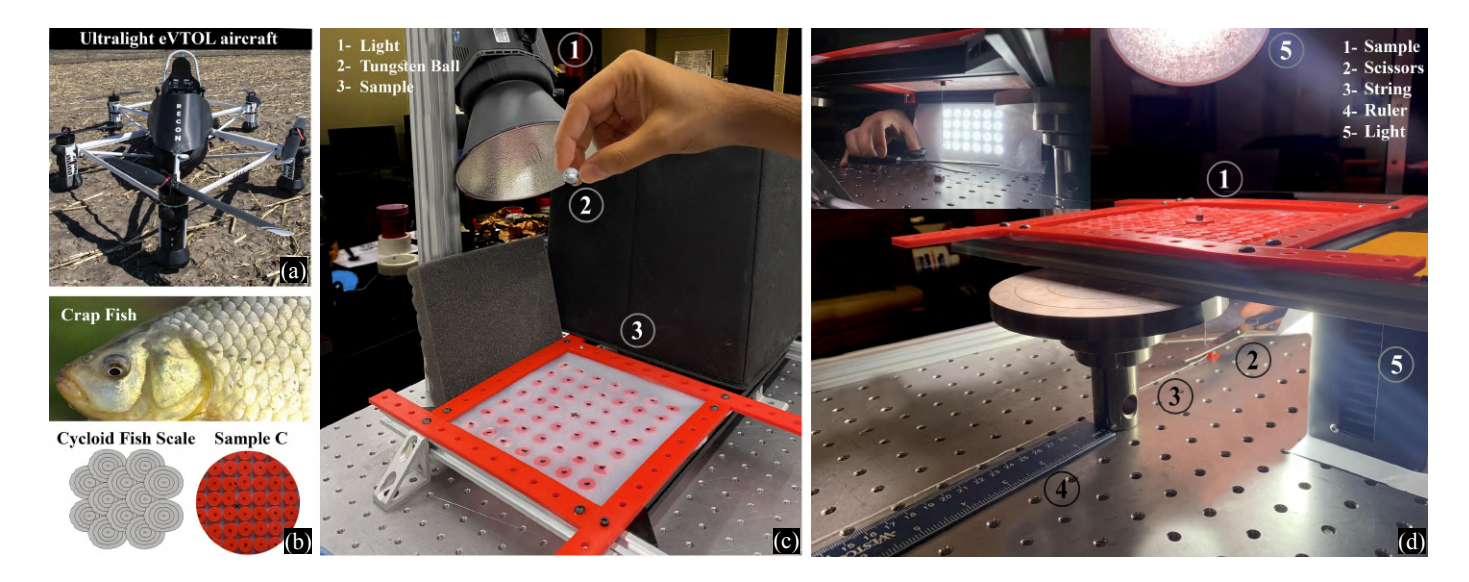


**FIGURE 1**. a) eVTOL aircraft [5], where scales covered membrane has potential use, b) illustration of crucian carp fish (right) [6], cycloid fish scale (left) [7], and pillar structure (bottom), c) and d) details of experimental setup for impact damping and free damping respectively.

advanced technologies in enhancing our understanding of structural dynamics [17, 18].

Substrates adorned with scales, drawing inspiration from biological structures, are consistently examined as a structural foundation exhibiting distinctive property amalgamations reminiscent of metamaterials. These systems consist physically of a substrate, incorporating protruding rigid plates that function as scales. The unique properties arise from the interplay of geometry and kinematics as scales slide across the substrate [19, 20]. We introduce a novel metamaterial characterized by a pillar structure inspired by the scales of fish. Recent investigations have explored the dynamic properties of thin plates and membranes inspired by fish scales [21]. In these studies, damping primarily arises from the sliding motion of the scales.

In this study, through a comprehensive analysis, we aim to unravel the damping characteristics of a membrane surface covered by pillars/scales, exploring two distinct scenarios of loading. The first scenario involves analyzing the impact response of the metasurface under a low-velocity impact load. In the second scenario, the membrane's mid-point undergoes an initial displacement via a string mechanism; subsequently, upon releasing the string, the free vibration response of the membrane is observed.

# 2 MATERIALS AND METHOD

To prepare the experimental sample, we used a widely available 3D printing mechanism. The vibration response is captured using high-speed cameras. A tungsten ball and a string are also used for vibrating the sample in two different scenarios. Finally, data are collected using Tracker software.

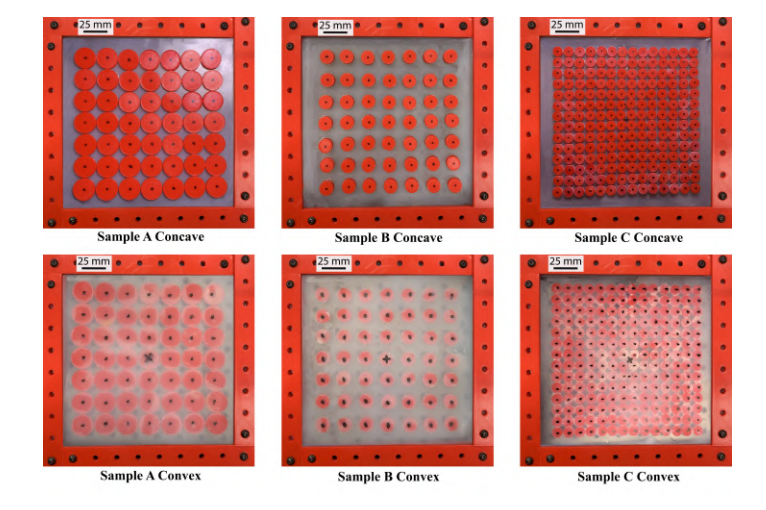


**FIGURE 2.** Experimental samples of scaled membrane structure including silicone membrane, rigid pillars, and clamps to the imposition of boundary conditions for concave and convex sides of the sample

# 2.1 SAMPLE PREPARATION

For fabricating scale-covered thin plates, using a 3D printer (Ultimaker US5) we created the mold for the membrane. Later we used dragon skin 10 material with a 1:1 ratio of curing agent to cast the membrane into the mold. Later, based on the different sample requirements we 3D print the pillars (to fabricate similar to scale-covered material). Pillars were made of Ultimaker Tough PLA ( $\sim 3GPa$ ) material. Finally, the pillar was glued into the membrane with a uniform distribution similar to the tetragonal lattice system of a square lattice. The samples are shown



**FIGURE 3**. Details regarding the equipment needed for the experiment

**TABLE 1**. Details of the samples used in this study.

Sample	R (mm)	H (mm)	S (mm)	Weight (gm)
A	12	3	1	152.1
В	8	6.75	5	149.7
С	5.75	3.25	1	153.3

in Fig. 2, here we consider the side in which button is places as concave and the reverse side as convex while the loading are applied. We have chosen the dimension of the pillar so that the total volume ( $V_P = \pi R^2 H$ ) of the sample and the total weight of the sample remain the same. We measure the weight of the pillar using a scale to ensure that pillars have similar weights it is needed. Only the number of contact points of the pillar is different.

Table 1 outlines the distinctive properties of the different samples. The radius (R) of the pillar for samples A, B, and C is 12 mm, 8 mm, and 5.75 mm respectively. Additionally, the height (H) of samples A, B, and C is 3 mm, 6.75 mm, and 3.25 mm respectively, while the gap or spacing (S) between the pillars measures 1 mm, 5 mm, and 1 mm respectively.

#### 2.2 EXPERIMENTAL ANALYSIS

We used two methods to investigate the vibration and damping of the samples. The first method involves using the diameter of 17.2 mm tungsten ball and allowing it to fall from 320 mm height toward the center of the scaled membrane structure with initial velocity ( $V_i = 0$ ), as observable in Fig. 1 (c). This creates the impact on the membrane as  $1/2mv^2$ , where the ball weight is m = 13.4 gm. The second method involves using a string, cre-

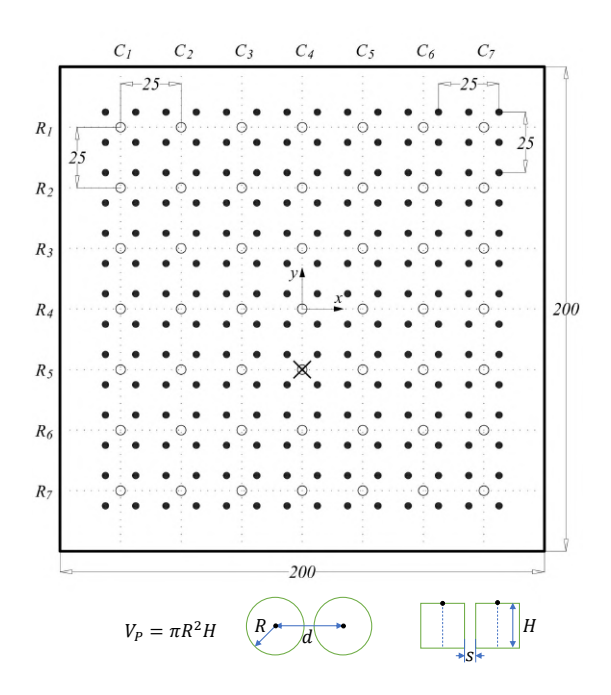


**FIGURE 4.** Details related to the dimensions of the sample, the placement of pillars in each of the samples A, B (hollow circle), and C (solid circle), as well as the target point (cross mark) to measure displacement and investigation of damping for impact loading and displacement from the center of the sample for initial displacement loading. [Dimensions are in mm]

ating 20 mm displacement at the center of the sample, and then abruptly cutting it, as clearly indicated in Fig. 1 (d).

All the samples were clamped in between the 3D printed clamping bar and metal bar with the use of screws in the four corners (Fig. 4). Finally, we mounted the clamping system into an optical table. The lighting system and high-speed camera were set up properly to capture the video from the top view and side view of the samples. The video capturing was recorded for all different samples in the concave and convex sides of the sample using Photron FASTCAM Mini AX100. We capture the video with 1000 fps focusing on the sample and having proper light. (Fig. 3)

We used open-source tracker software to collect data from each sample. As shown in Fig. 4, to specify the specific point during data acquisition we divided the samples into seven columns and seven rows. In the sample, each point is in 25 mm distance incrementally from the center of the point. The data collection procedure comprised the initial step of importing the video into the software, followed by the configuration of the calibration stick and axis within the samples. Subsequently, we selected the desired points and established a template within the software designed for optimal auto-tracking of these points. Finally, we visually checked the software to identify and rectify any

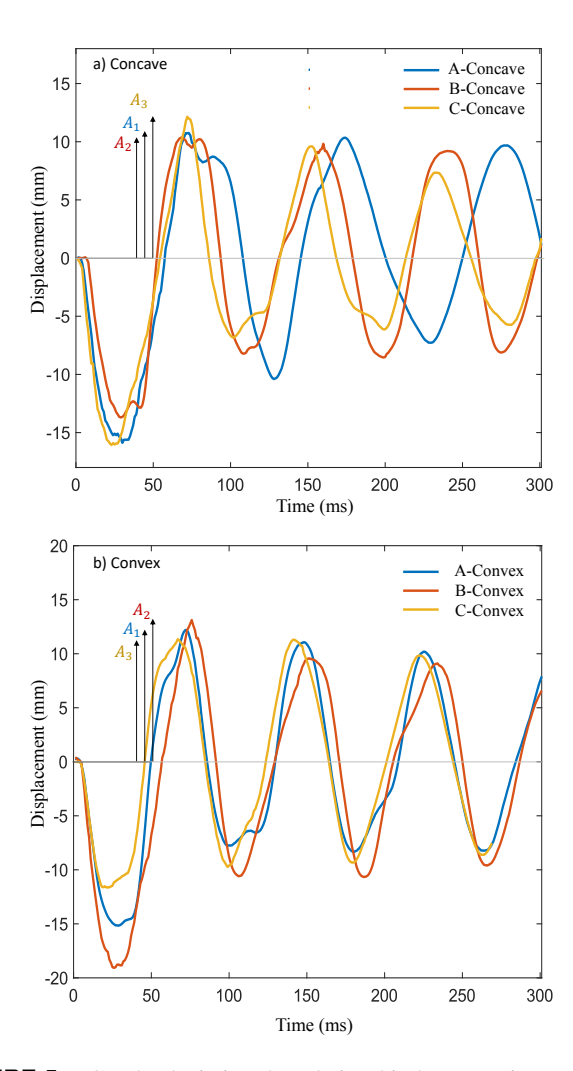


**FIGURE 5**. Graphs depicting the relationship between time and displacement are presented for both the concave and convex sides of the sample in response to impact loading.

errors during the auto-tracking of the point. In the impact test, data was recorded from C4R5 since tracking the middle point was challenging due to it being obscured by the ball during impact. Conversely, for the displacement test, data was obtained from the middle point (C4R4) as there were no obstacles hindering data collection from this location. The data was collected from both the middle point and the nearest possible alternative middle point to ensure the acquisition of optimal data for subsequent damping analysis. To compute the damping ratio, we first evaluate the logarithmic decrement ( $\delta$ ) using the formula, where  $A_n$  is the amplitude of one peak and  $A_{n+k}$  is the amplitude of the next peak:

$$\delta = \ln\left(\frac{A_n}{A_{n+k}}\right)$$

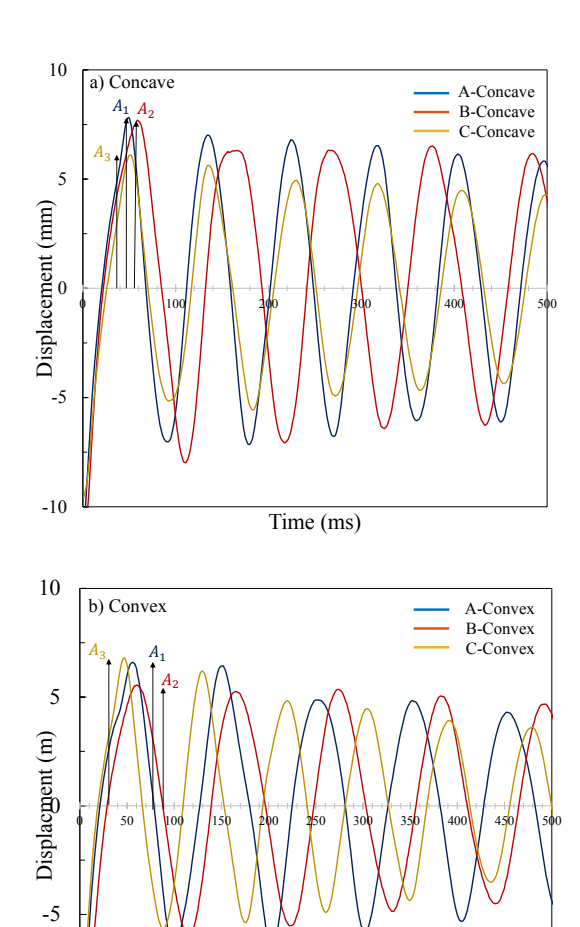


**FIGURE 6**. Graphs illustrating the relationship between time and displacement are presented for both the concave and convex sides of the sample, originating from a given initial displacement.

Time (ms)

Subsequently, the damping ratio ( $\zeta$ ) is determined as:

$$\zeta = rac{\delta}{\sqrt{4\pi^2 + \delta^2}}$$

We conducted the damping analysis for various peaks until 3000 ms, ultimately obtaining the average damping within this time frame for each test.

# 3 RESULTS AND DISCUSSION

-10

In investigating the damping behavior through impact tests, it becomes evident that the initial displacement remains consistent for the concave loading condition. Examining Fig. 5 reveals varying amplitude reductions for each configuration, with

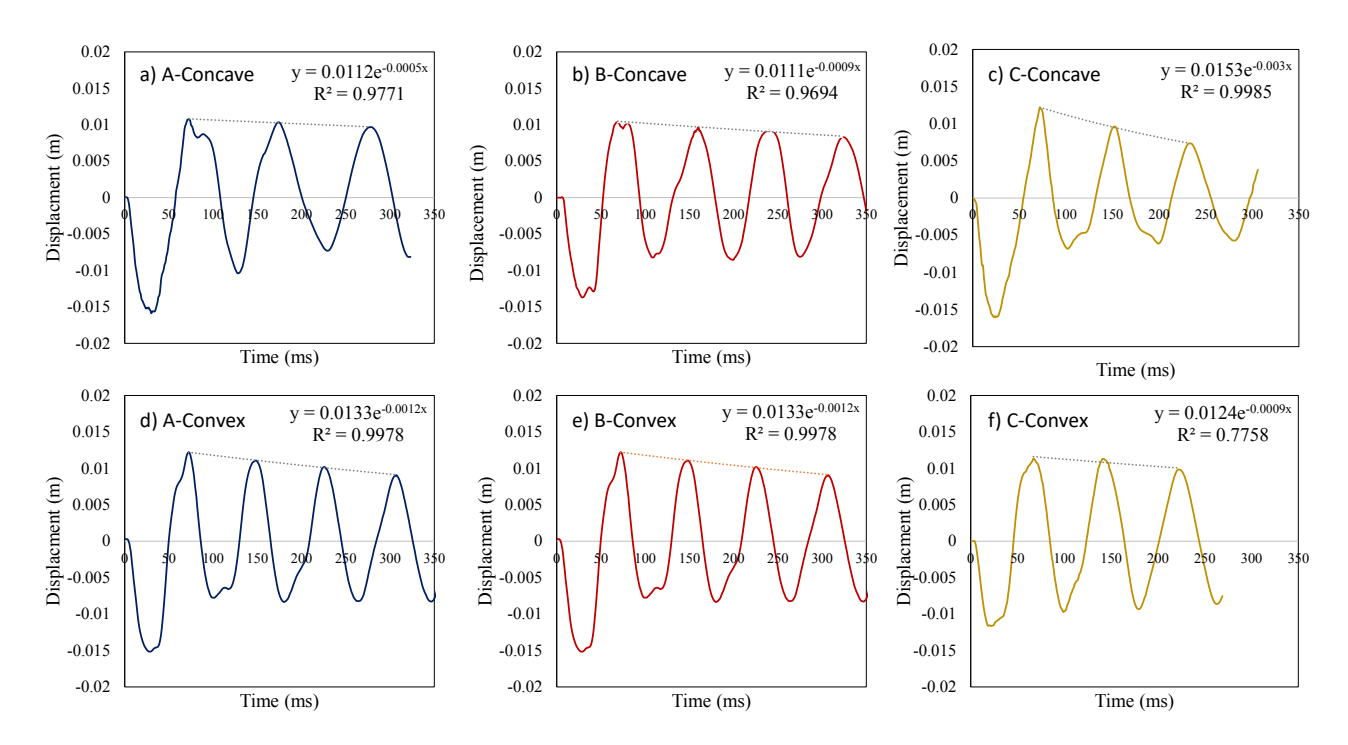


**FIGURE 7**. The behavior of point C4R5 on the pillar/scaly viscoelastic plate varies with different pillar contact orientations under impact loads. Panels a) to c) illustrate the response to concave impact, while panels d) to f) depict the behavior of convex samples.

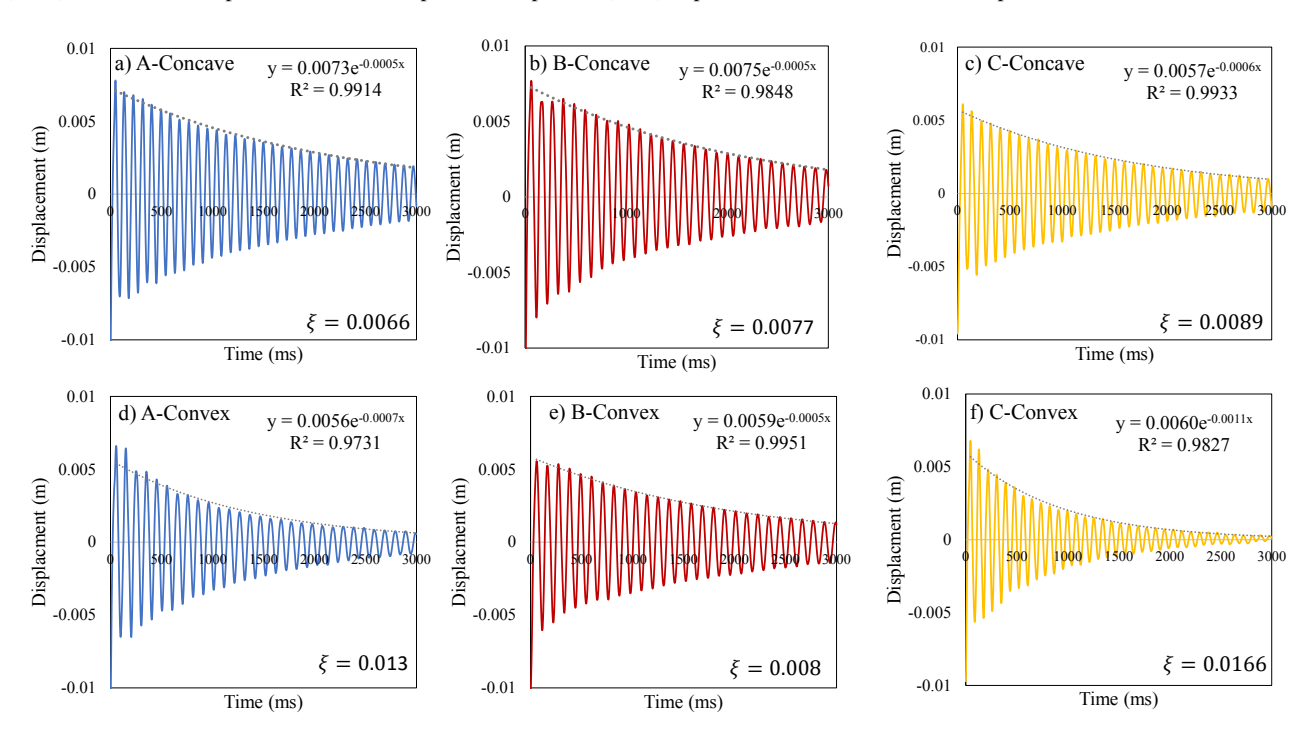


**FIGURE 8**. The behavior of the middle point (C4R4) on the viscoelastic plate with pillar/scaly structure varies under displacement loads for different pillar contact orientations. Panels a) to c) depict the response for concave samples, while panels d) to f) illustrate the behavior for convex samples.

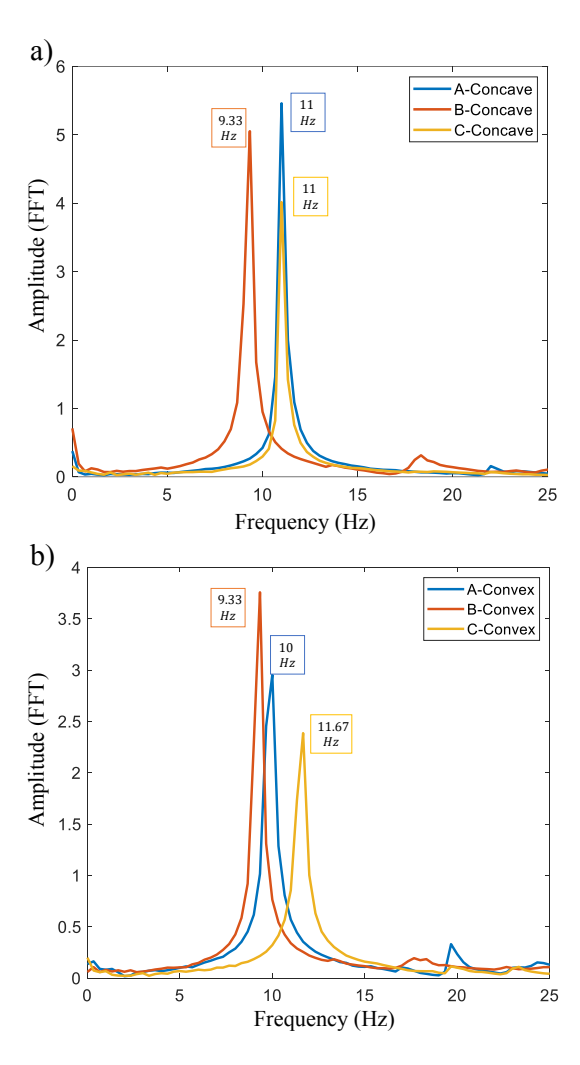
notably minimal differences between samples in the convex loading scenario.

Fig. 7 illustrates a pronounced damping effect for pillars with a lower radius, showcasing a higher pillar density compared to the other two samples. This observation strongly suggests that the damping capability of the plate covered with scales or pillars is contingent upon the number of collisions among the pillars. On the other hand, in convex loading during impact, the degree of contact has a lower impact on damping.

The study on pillar-covered plates reveals notable damping properties, particularly during ball impact. The damping characteristics exhibit persistence until the point when the ball returns to the membrane, initiating a subsequent impact, which changes the characteristics of damping in a different way. Our focus is on gathering data up to the moment just before the subsequent ball impact. To mitigate the influence of this phenomenon, we conduct an additional analysis of the damping behavior exhibited by pillar-covered structures. In this case, an initial displacement is induced into the membrane as described earlier in the previous section. Examining Fig. 6, we observe that immediately after loading, the amplitude of sample-C is at its lowest in the concave sample, while the reverse holds true for the convex sample. Figure 8 further illustrates that irrespective of loading type (concave or convex), the pillar-covered sample with higher density exhibits greater damping than the other two samples. Notably, in both loading scenarios, sample B, where no contact exists between the pillars, demonstrates the lowest damping.

We conducted a Fast Fourier Transform (FFT) to delve deeper into the analysis of time versus displacement. As shown in Fig. 9, the frequency of the sample varies depending on the loading side (concave and convex), except for sample-B. The absence of interaction among pillars in sample B maintains a constant frequency. Among all the samples we found that FFT amplitude is higher for concave loading conditions. We also found that sample C shows lowest amplitude among all the samples for both loading conditions. Noteworthy is sample C, which demonstrates significant damping during convex loading, leading to the lowest amplitude for this sample. Besides, the FFT also demonstrates that for concave loading sample A and sample B having almost similar amplitude but during convex loading sample A (which has more damping) show lower FFT amplitude than sample B. This analysis underscores the significant influence of the number of pillar contacts during loading on the damping characteristics, providing insights into the diverse structures of the membranes studied.

For analyzing scale/pillar-covered membrane further using a mathematical model, we used the viscous damping model to compare the damping of the structure for various structures for the initial displacement loading in the convex region [22].



**FIGURE 9**. Frequency vs amplitude (mm) distribution of samples depicting the concave and convex regions under displacement loading.

$$\frac{d^2x(t)}{dt^2} + \eta_A \omega_n^2 \frac{dx(t)}{dt} + \omega_n^2 x(t) = 0$$

The equation as a whole describes the balance between the acceleration, damping force, and spring force. In a damped harmonic oscillator, the damping term  $\eta_A \omega_n^2 \frac{dx(t)}{dt}$  is responsible for modeling the dissipation of energy from the system, leading to a gradual decrease in amplitude over time, here  $\eta_A$  is damping constant. The larger the damping constant  $\eta_A$ , the faster the energy dissipates, and the quicker the oscillations decay. The solution to this differential equation provides the displacement x(t) as a function of time, and it characterizes the damped oscillatory behavior of the system. Where,  $\frac{d^2x(t)}{dt^2}$ : This term represents the

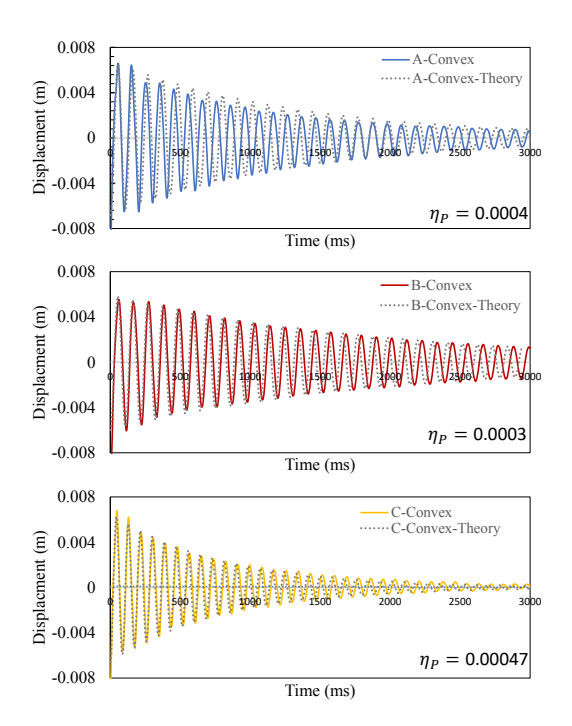


**FIGURE 10**. Frequency vs amplitude (mm) distribution of samples depicting the convex regions under displacement loading.

acceleration of the system,  $\omega_n$  is the natural frequency, and  $\frac{dx(t)}{dt}$  is the velocity of the system.

In our investigation, comparing with the mathematical model, we used the frequency (f) that we achieved using FFT to calculate the natural frequency using,  $\omega_n = 2\pi f$ . Later using,  $\omega_n$ , initial displacement  $(x_0)$  of the first positive peak for different signals, and unique damping constant for each signal we found an excellent match with our experimental result, which is illustrated in Figure 10. Notably, we observed the highest damping constant  $(\eta_A = 0.00047)$  at the point of contact for sample C. Conversely, sample B, where there is no contact between the pillars, exhibited the lowest damping constant  $(\eta_A = 0.0003)$ . This reaffirms that the contact pillar significantly influences the damping properties of the substrate covered by the scale.

# 4 CONCLUSION

In this investigation, an exhaustive examination of a pillar/scale-covered membrane was conducted. The study commenced with the fabrication of distinct samples, followed by a series of experimental tests encompassing impact and displacement assessments. The outcomes of these experiments revealed diverse damping properties exhibited by the samples. The investigation specifically delved into damping asymmetries between concave and convex loading curvatures, maintaining consistent overall sample mass. The study scrutinized the differen-

tial damping responses under impact loading conditions for each case. In the analytical process for the initial displacement loading conditions, aside from contrasting damping characteristics, a detailed signal analysis was employed to investigate frequency variations, elucidating differences through the employment of the FFT method. Furthermore, the damping profiles resulting from initial displacement loading conditions were fitted with an existing model to establish connections between the metasurface architecture and its damping behavior. Based on the investigation, it was observed that among the three distinct samples, Sample C exhibited superior damping properties in comparison to the other two specimens for both impact and initial displacement loading. In contrast, Samples A and B demonstrated minimal damping, likely attributed to the reduced contact effects between buttons due to differences in dimensions and the quantity of buttons in place.

Further investigations into the scale-covered metastructure can advance the development of a comprehensive mathematical model by exploring additional damping and vibration properties. This involves a detailed examination and potential refinement of the mathematical framework to encompass a broader range of parameters and conditions. Such research efforts promise to provide valuable insights to enhanced understanding and potential applications in engineering and materials science.

# **ACKNOWLEDGMENT**

This work was supported by the United States National Science Foundation's Civil, Mechanical, and Manufacturing Innovation, Grant No. 2028338.

#### **REFERENCES**

- [1] Abdulameer, H. A., and Wasmi, H. R., 2015. "Vibration control analysis of aircraft wing by using smart material". *Innovative Systems Design and Engineering*, **6**(8), pp. 7–42.
- [2] Sharma, K., and Srinivas, G., 2020. "Flying smart: Smart materials used in aviation industry". *Materials Today: Proceedings*, 27, pp. 244–250.
- [3] Jiakun, H., Zhe, H., Fangbao, T., and Gang, C., 2021. "Review on bio-inspired flight systems and bionic aerodynamics". *Chinese Journal of Aeronautics*, *34*(7), pp. 170–186.
- [4] Aeroelasticity, F. E. "Introduction to structural dynamics and aeroelasticity".
- [5] of Agriculture, U. D., 2010 (accessed November 14, 2023). evtol aircraft. Online Image, Flickr, https: //tinyurl.com/rcrv3btd.
- [6] M.shattock, 2010 (accessed November 14, 2023). Crucian carp fish. Online Image, Flickr, https://tinyurl.com/44mnwvzk.

- [7] Waters, N., 2010 (accessed November 14, 2023). Cycloid fish scales. Online Image, Flickr, https://tinyurl.com/nhfvndwm.
- [8] Jenkins, C. H., and Korde, U. A., 2006. "Membrane vibration experiments: An historical review and recent results". *Journal of Sound and Vibration*, **295**(3-5), pp. 602–613.
- [9] Zheng, Z.-L., Liu, C.-J., He, X.-T., and Chen, S.-L., 2009. "Free vibration analysis of rectangular orthotropic membranes in large deflection.". *Mathematical Problems in Engineering*, 2009.
- [10] Ouakad, H. M., 2019. "Free vibration characteristics of rectangular membranes assuming rounded-edges boundary". *Vibration*, 2(3), pp. 265–270.
- [11] Bauer, L., and Reiss, E. L., 1973. "Free vibrations of rhombic plates and membranes". *The Journal of the Acoustical Society of America*, *54*(5), pp. 1373–1375.
- [12] Lima-Rodriguez, A., Gonzalez-Herrera, A., and Garcia-Manrique, J., 2019. "Study of the dynamic behaviour of circular membranes with low tension". *Applied Sciences*, 9(21), p. 4716.
- [13] Filipich, C. P., and Rosales, M. B., 2007. "Vibration of non-homogeneous rectangular membranes with arbitrary interfaces". *Journal of sound and vibration*, *305*(4-5), pp. 582–595.
- [14] Kang, S. W., 2004. "Free vibration analysis of composite rectangular membranes with a bent interface". *Journal of Sound and Vibration*, 272(1-2), pp. 39–53.
- [15] Abdulkerim, S., Dafnis, A., and Riemerdes, H.-G., 2019. "Experimental investigation of nonlinear vibration of a thin rectangular plate". *International Journal of Applied Mechanics*, 11(06), p. 1950059.
- [16] Lu, T., Shen, H.-S., Wang, H., Chen, X., and Feng, M., 2023. "Linear and nonlinear free vibration and optimal design of bio-inspired helicoidal cfrpc laminated plates". *In*ternational Journal of Structural Stability and Dynamics, p. 2450098.
- [17] Yu, L., and Pan, B., 2017. "Single-camera high-speed stereo-digital image correlation for full-field vibration measurement". *Mechanical Systems and Signal Processing*, *94*, pp. 374–383.
- [18] Tomac, I., and Slavič, J., 2022. "Damping identification based on a high-speed camera". *Mechanical Systems and Signal Processing*, **166**, p. 108485.
- [19] Ali, H., Ebrahimi, H., and Ghosh, R., 2019. "Frictional damping from biomimetic scales". *Scientific reports*, **9**(1), p. 14628.
- [20] Hossain, M. S., Ebrahimi, H., and Ghosh, R., 2022. "Fish scale inspired structures-a review of materials, manufacturing and models". *Bioinspiration & Biomimetics*.
- [21] Ebrahimi, H., Krsmanovic, M., Ali, H., and Ghosh, R., 2023. "Material-geometry interplay in damping of biomimetic scale beams". *arXiv* preprint

- arXiv:2303.04920.
- [22] Zhang, W., and Simizu, N., 1999. "Damping properties of the viscoelastic material described by fractional kelvin-voigt model". *JSME International Journal Series C Mechanical Systems, Machine Elements and Manufacturing*, 42(1), pp. 1–9.